*Inorg. Chem.* **2008**, *47*, 2661−2667

# Structure and Electrons in Mayenite Electrides

**Luis Palacios**,[†] **Aurelio Cabeza**,[†] **Sebastián Bruque**,[†] **Santiago García-Granda**,[‡] **and Miguel A. G. Aranda***,[†]

*Departamento de Química Inorgánica, Cristalografía y Mineralogía, Universidad de Málaga, 29071 Málaga, Spain, and Departamento de Química Física y Analítica, Universidad de Oviedo, c/Julián Clavería, 33006 Oviedo, Spain*

Received October 26, 2007

One major goal in materials chemistry is to find inexpensive compounds with improved capabilities. Stable inorganic electrides, derived from nanoporous mayenite $[Ca_{12}Al_{14}O_{32}]O$, are a new family that has very interesting properties such as electronic conductivity combined with transparency. However, an intriguing fundamental problem is to understand the structures of these cubic materials and to characterize their free-electron loadings. Here we report an accurate structural study for three members of the series $[Ca_{12}Al_{14}O_{32}]O_{1-\delta}e_{2\delta}$ ($\delta = 0$, 0.15, and 0.45), from single-crystal low-temperature synchrotron X-ray diffraction. The complex structural disorder imposed by the presence of the oxide anions into the mayenite cages has been unravelled. Furthermore, the final electron density map for $\delta = 0.45$ black mayenite has shown electron density localized into the center of the cages, which is the first experimental proof of their electride nature. The reported structural findings challenge theorists to improve predictive models in this new family of materials.

## Introduction

Trapping of electrons in a stoichiometric composition in the solid state has provided a family of compounds called electrides, where the electrons are occupying anionic sites.[1] Thermoionic power generation and cold-cathode electron-field emission have been some of the potential applications proposed for such materials.[2] However, organic electrides[3] have prevented any practical application because of their lack of stability at room temperature, with the exception of a recently synthesized compound.[4] Thus, the search for inorganic electrides, where the electron anion locates inside the cavities of an inorganic matrix, has become important for practical profit of the properties of the trapped electrons. The nanoporous oxide mayenite provides a structure in which oxide anions can be partially replaced by electrons, with thermal stability, even under ambient atmosphere.[5] The electronic properties of these electrides range from superconductivity, at high electron contents,[6] to semiconductivity, at low electron loadings.[7] They can even combine electronic conductivity and transparency, which is very useful for flat displays and electronic devices.[8,9] There have been many different theoretical approaches to developing a model for the electronic structure consistent with the amazing properties of this family of electrides.[10–14]

* To whom correspondence should be addressed. E-mail: g_aranda@uma.es.
[†] Universidad de Málaga.
[‡] Universidad de Oviedo.

(1) Dye, J. L. *Science* **2003**, *301*, 607–608.
(2) Phillips, R. C.; Pratt, W. P.; Dye, J. L. *Chem. Mater.* **2000**, *12*, 3642–3647.
(3) Wagner, M. J.; Huang, R. H.; Eglin, J. L.; Dye, J. L. *Nature* **1994**, *368*, 726–729.
(4) Redko, M. Y.; Jackson, J. E.; Huang, R. H.; Dye, J. L. *J. Am. Chem. Soc.* **2005**, *127*, 12516–12422.
(5) Matsuishi, S.; Toda, Y.; Miyakawa, M.; Hayashi, K.; Kamiya, T.; Hirano, M.; Tanaka, I.; Hosono, H. *Science* **2003**, *301*, 626–629.
(6) Miyakawa, M.; Kim, S. W.; Hirano, M.; Kohama, Y.; Kawaji, H.; Atake, T.; Ikegami, H.; Kono, K.; Hosono, H. *J. Am. Chem. Soc.* **2007**, *129*, 7270–7271.
(7) Kamiya, T.; Aiba, S.; Miyakawa, M.; Nomura, K.; Matsuishi, S.; Hayashi, K.; Ueda, K.; Hirano, M.; Hosono, H. *Chem. Mater.* **2005**, *17*, 6311–6316.
(8) Hayashi, K.; Matsuishi, S.; Kamiya, T.; Hirano, M.; Hosono, H. *Nature* **2002**, *419*, 462–465.
(9) Medvedeva, J. E.; Freeman, A. J. *Europhys. Lett.* **2005**, *69*, 583–587.
(10) Sushko, P. V.; Shluger, A. L.; Hayashi, K.; Hirano, M.; Hosono, H. *Phys. Rev. Lett.* **2003**, *91*, 126401.
(11) Medvedeva, J. E.; Freeman, A. J.; Bertoni, M. I.; Mason, T. O. *Phys. Rev. Lett.* **2004**, *93*, 016408.
(12) Li, Z. Y.; Yang, J. L.; Hou, J. G.; Zhu, Q. S. *Angew. Chem., Int. Ed.* **2004**, *43*, 6479–6482.
(13) Sushko, P. V.; Shluger, A. L.; Hayashi, K.; Hirano, M.; Hosono, H. *Phys. Rev. B* **2006**, *73*, 045120.
(14) Sushko, P. V.; Shluger, A. L.; Hirano, M.; Hosono, H. *J. Am. Chem. Soc.* **2007**, *129*, 942–951.

10.1021/ic7021193 CCC: $40.75 
Published on Web 02/19/2008

Mayenite, $12CaO \cdot 7Al_2O_3$ (C12A7), is an important phase of calcium aluminate cements. Its cubic structure, $I\bar{4}3d$ space group, with a lattice constant of ~11.99 Å and a unit cell content of $Ca_{24}Al_{28}O_{66}$, was refined from single-crystal data as early as 1970,[15] and it has been very recently revisited by high-temperature neutron powder diffraction.[16] The unit cell structural formula of stoichiometric mayenite can be expressed as $[Ca_{24}Al_{28}O_{64}]^{4+}\square_{10}2O^{2-}$ and it has been considered as an antizeolite framework formed by 12 positively charged cages where 2 extraframework oxide anions are statistically distributed to compensate for the framework charge. The low occupation of the cages renders a number of properties for functional applications such as oxide conductivity,[17] catalysis,[18] and anion exchange at high temperatures. It has been found that those oxide anions can be replaced by a large variety of anionic species, $O_2^-$,[19] $O_2^{2-}$,[20] $O^-$,[21] $OH^-$,[22] $H^-$,[8] and $e^-$ (electride).[5]

The gradual replacement of the oxide anions located in the cages by electrons has provided the series $[Ca_{12}Al_{14}O_{32}]^{2+}\square_{5-\delta}O^{2-}_{1-\delta}e^-_{2\delta}$ ($0 \le \delta \le 1$) ranging from $\delta = 0$ in the white room-temperature insulating oxymayenite, $[Ca_{12}Al_{14}O_{32}]^{2+}\text{-}\square_5O^{2-}$, to $\delta = 1$ in the black metallic-conducting electride, $[Ca_{12}Al_{14}O_{32}]^{2+}\square_4e^-_2$, being green for low electron loadings. An insulator–metal transition has been very recently reported in this series with a sharp enhancement of the electron drift mobility from ~0.1 to 4 $cm^2\ V^{-1}\ s^{-1}$.[23] So far, four methods[24] have been reported to prepare these electron-loaded main-element oxides: (i) metal treatment (Ca,[5] Ti,[23] and V[25]) under very low pressures; (ii) reaction with hydrogen gas at high temperature followed by UV-light illumination, which produces the photodissociation of the occluded hydride anions and the release of electrons into the cages;[8,26] (iii) direct solidification of a graphite-reduced C12A7 melt,[27] followed by crystallization of the transparent glass; (iv) treatment of C12A7 powders at high temperature (1000–1200 °C) under a $CO/CO_2$-rich atmosphere.[28] It must be noted that the electride formation can be followed in situ, at high temperatures and low pressures, using neutron powder diffraction.[25]

The electronic structure of mayenite electrides has been the subject of controversy in different theoretical studies. The earlier approaches[10] developed an electride model in which the electon density was mainly localized in the cages; a later work[11] presented a model with a highly delocalized electron density penetrating the regions occupied by cations, thus being in contradiction with the electride model. A subsequent study provided a model with localized electrons but without being stoichiometric.[12] The most recent model[14] has stated that the electronic structure changes with the electron concentration, $2\delta$, but they are neither associated with specific atoms nor fully delocalized. At sufficiently high values of $2\delta$, the system becomes metallic but still retains the partially localized character of the conducting electrons.

The main aim of this work was to determine the crystal structures of electron-loaded mayenites below the critical electron concentration in which the metal−semiconductor transition occurs,[23] in order to understand the complex disorder and properties of these compounds. To do so, outstanding single-crystal low-temperature synchrotron X-ray diffraction data have been collected for three samples. These data, analogous to those collected for charge density studies, have allowed characterization of the structures and, furthermore, visualization of the "free"-electron position in black $Ca_{12}Al_{14}O_{32.55}e_{0.9}$.

## Results and Discussion

Single crystals were prepared as described in the Experimental Section. A photograph of the crystals with different electron loadings is shown in Figure 1. The evolution of color perfectly agrees with that of previous reports.[5,8,23] The structural study is based on synchrotron X-ray diffraction data (see the Experimental Section), and data collection details are given in Table 1. The electride structural description reported in our previous single-crystal study[25] was based on 422 reflections (393 observed with $I > 2\sigma(I)$; 0.71 Å resolution limit) from laboratory X-ray data (Mo Kα). For the present study, much better diffraction data have been collected. It must be underlined that the structures reported here are based on 1640 unique reflections (averaged out from more than 30 000 measured reflections), with more than 1600 being considered as observed (criterion: $I > 4\sigma(I)$; 0.45 Å resolution limit). Furthermore, low-temperature data, 90 K, were collected in order to minimize the thermal vibration contribution to the anisotropic atomic displacement parameters, ADPs. By way of this procedure, the local positional disorder could be determined because its relative contribution to the total scattering power is larger.

The basic structural unit of the mayenite framework is the cage depicted in Figure 2 (top). In the absence of deforma-


(15) Bartl, H.; Scheller, T. *Neues Jahrb. Mineral., Monatsh.* **1970**, *35*, 547–552.
(16) Boysen, H.; Lerch, M.; Stys, A.; Senyshyn, A. *Acta Crystallogr., Sect. B* **2007**, *63*, 675–682.
(17) Lacerda, M.; Irvine, J. T. S.; Glasser, F. P.; West, A. R. *Nature* **1988**, *332*, 525–526.
(18) Wang, Z.; Pan, Y.; Dong, T.; Zhu, X.; Kan, T.; Yuan, L.; Torimoto, Y.; Sadakata, M.; Li, Q. *Appl. Catal., A* **2007**, *320*, 24–34.
(19) (a) Hosono, H.; Abe, Y. *Inorg. Chem.* **1987**, *26*, 1192–1195. (b) Matsuishi, S.; Hayashi, K.; Hirano, M.; Tanaka, I.; Hosono, H. *J. Phys. Chem. B* **2004**, *108*, 18557–18568.
(20) (a) Hayashi, K.; Hirano, M.; Hosono, H. *Chem. Lett.* **2005**, *34*, 586–587. (b) Kajihara, K.; Matsuishi, S.; Hayashi, K.; Hirano, M.; Hosono, H. *J. Phys. Chem. C* **2007**, *111*, 14855–14861.
(21) Hayashi, K.; Matsuishi, S.; Hirano, M.; Hosono, H. *J. Phys. Chem. B* **2004**, *108*, 8920–8925.
(22) (a) Li, J.; Huang, F.; Wang, L.; Yu, S. Q.; Torimoto, Y.; Sadakata, M.; Li, Q. X. *Chem. Mater.* **2005**, *17*, 2771–2774. (b) Nomura, T.; Hayashi, K.; Kubota, Y.; Kamiya, T.; Hirano, M.; Takata, M.; Hosono, H. *Chem. Lett.* **2007**, *36*, 902–903.
(23) Kim, S. W.; Matsuishi, S.; Nomura, T.; Kubota, Y.; Takata, M.; Hayashi, K.; Kamiya, T.; Hirano, M.; Hosono, H. *Nano Lett.* **2007**, *7*, 1138–1143.
(24) Kim, S. W.; Matsuishi, S.; Miyakawa, M.; Hayashi, K.; Hirano, M.; Hosono, H. *J. Mater. Sci.: Mater. Electron.* **2007**, *18*, S5–S14.
(25) Palacios, P.; De La Torre, A. G.; Bruque, S.; Garcia-Muñoz, J. L.; Garcia-Granda, S.; Sheptyakov, D.; Aranda, M. A. G. *Inorg. Chem.* **2007**, *46*, 4167–4176.
(26) Hayashi, K.; Sushko, P. V.; Shluger, A. L.; Hirano, M.; Hosono, H. *J. Phys. Chem. B* **2005**, *109*, 23836–23842.
(27) Kim, S. W.; Toda, Y.; Hayashi, K.; Hirano, M.; Hosono, H. *Chem. Mater.* **2006**, *18*, 1938–1944.
(28) Kim, S. W.; Hayashi, K.; Hirano, M.; Hosono, H.; Tanaka, I. *J. Am. Ceram. Soc.* **2006**, *89*, 3294–3298.


**Figure 1.** Photograph of mayenite crystals and the titanium container. From top to bottom are shown crystals with increasing electron loadings, and therefore different colors. The single-crystal data were collected for (i) transparent colorless C12A7 (top) and (ii) transparent green C12A7-eg (intermediate) and opaque black C12A7-eb (bottom).

**Table 1.** Crystallographic Details, Data Collection, and Refinement Results for Studied Mayenite Structures

| | C12A7 | C12A7-eg | C12A7-eb |
|---|---|---|---|
| *T*/K | 90 | 90 | 90 |
| wavelength/Å | 0.724 434 | 0.724 434 | 0.724 434 |
| cell parameter *a*/Å | 11.97113(8) | 11.97699(7) | 11.99580(7) |
| cell volume/Å$^3$ | 1715.56(1) | 1718.08(1) | 1726.19(1) |
| calcd density/g cm$^{-3}$ | 2.68 | 2.68 | 2.67 |
| abs coeff/mm$^{-1}$ | 2.28 | 2.28 | 2.27 |
| *F*(000) | 1371.8 | 1371.8 | 1371.8 |
| cryst size/mm$^3$ | 0.10 × 0.05 × 0.04 | 0.10 × 0.08 × 0.05 | 0.07 × 0.06 × 0.05 |
| cryst color | colorless | pale green | black |
| $\theta$ range/deg | 4.3–53.5 | 4.3–53.5 | 4.2–53.3 |
| limiting indices | $-23 \le h \le 23$<br>$-26 \le k \le 26$<br>$-26 \le l \le 26$ | $-23 \le h \le 23$<br>$-26 \le k \le 26$<br>$-26 \le l \le 26$ | $-26 \le h \le 24$<br>$-26 \le k \le 23$<br>$-22 \le l \le 26$ |
| reflns overall/unique | 33332/1647 | 30347/1638 | 32992/1648 |
| data range/Å | 0.45–6.2 | 0.45–6.2 | 0.45–6.2 |
| *R*(int) | 0.0548 | 0.0503 | 0.0543 |
| $R(\sigma)$ | 0.0175 | 0.0169 | 0.0183 |
| data/restraints/param | 1647/4/38 | 1638/4/37 | 1648/4/37 |
| refinement threshold | $F_o > 4\sigma(F_o)$ | $F_o > 4\sigma(F_o)$ | $F_o > 4\sigma(F_o)$ |
| data > threshold | 1647 > 1634 | 1638 > 1617 | 1648 > 1601 |
| GOF | 1.1480 | 1.1020 | 1.1080 |
| R1(obs) | 0.0208 | 0.0303 | 0.0252 |
| R1(all) | 0.0210 | 0.0307 | 0.0259 |
| wR2 | 0.0532 | 0.0823 | 0.0625 |
| highest peak/e Å$^{-3}$ | 0.64 | 1.43 | 0.79 |
| deepest hole/e Å$^{-3}$ | −0.48 | −0.42 | −0.47 |

tion/disorder induced by the extraframework specie(s), e.g., oxide anions, the framework belongs to the $I\bar{4}3d$ space group and the cages have $S_4$ symmetry. However, the anions located inside the cages to counterbalance the charge are disordered over the available cages and perturb the lattice; thus, the $S_4$ symmetry is preserved only on average. One oxide anion at the center of a cage would be coordinated to two calcium cations at 2.83 Å and four aluminum cations at 3.47 Å (see Figure 2, top). The bond valence sum[29] resulting from this

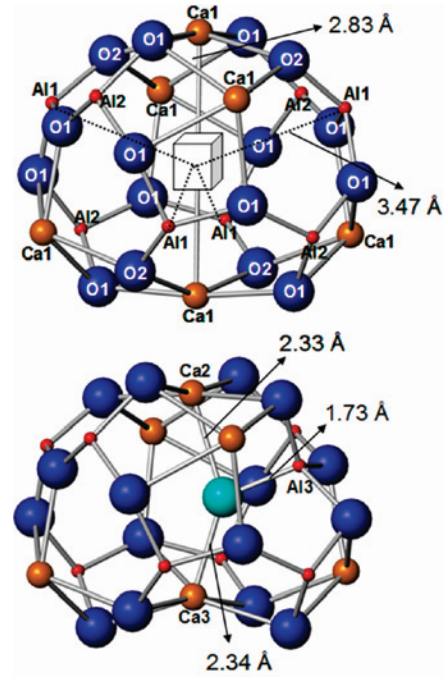


**Figure 2.** Ball-and-stick view of mayenite cages in $[Ca_{12}Al_{14}O_{32}]^{2+}\text{-}\square_{5-\delta}O^{2-}{}_{1-\delta}e^{-}{}_{2\delta}$. Top: undeformed empty cage. The atoms have been labeled, and the closest interatomic distances to the center of the cage are given. Bottom: deformed filled cage due to the "extraframework" oxide anions, O3o (light blue). O3o is located out of the center of the cage, and it provokes the movement (positional disorder) of the Ca1 cations, yielding Ca2 and Ca3 sites (deformation along the $S_4$ axis). The presence of O3o also causes the movement of Al1, yielding Al3, which satisfies the O3o coordination requirements. The closest interatomic distances around O3o are given.

oxygen environment has a value of 0.20 valence units, far lower than that expected for conventional oxides. In other words, the diameter of the cage is so big, ~4.5 Å, that an oxide at the center of the cage is unstable.

Some intermediate models have already been proposed,[16,25,30] but they do not take into account all disorder present in the mayenite structures. The difference Fourier maps (see Figure 3, bottom) clearly give new peaks corresponding to a third calcium position, Ca3, a disorder aluminum, Al3, and electron density due to oxygen species in the center of the cages for C12A7. The effects of including these atoms in the structural models are given in the Supporting Information (Table S1). Table S1 gives the *R* factors of the different models plus the position and height of the most intense peaks in the difference Fourier maps. The evolution of the *R* factors with the inclusion of each new (disordered) atom is listed. The improvement in the fits to the diffraction data, corresponding to each structural description, can be seen as the *R* factors drop continuously. The *R* factors for the final models are given in Table 1.

The initial structural model used to unravel the local disorder in the $[Ca_{12}Al_{14}O_{32}]^{2+}\square_{5-\delta}O^{2-}{}_{1-\delta}e^{-}{}_{2\delta}$ series includes only Ca1, Al1, Al2, O1, and O2, which built up the undistorted cages,[15] and, initially, it neglects the extraframework oxide. The difference Fourier maps from this model are given in the top panels of Figure 3. Electron density peaks arising from disordered calcium atoms (labeled) are clearly

(29) Brown, I. D.; Altermatt, D. *Acta Crystallogr., Sect. B* **1985**, *41*, 244–247.

(30) Sushko, P. V.; Shluger, A. L.; Hayashi, K.; Hirano, M.; Hosono, H. *Phys. Rev. B* **2006**, *73*, 014101.

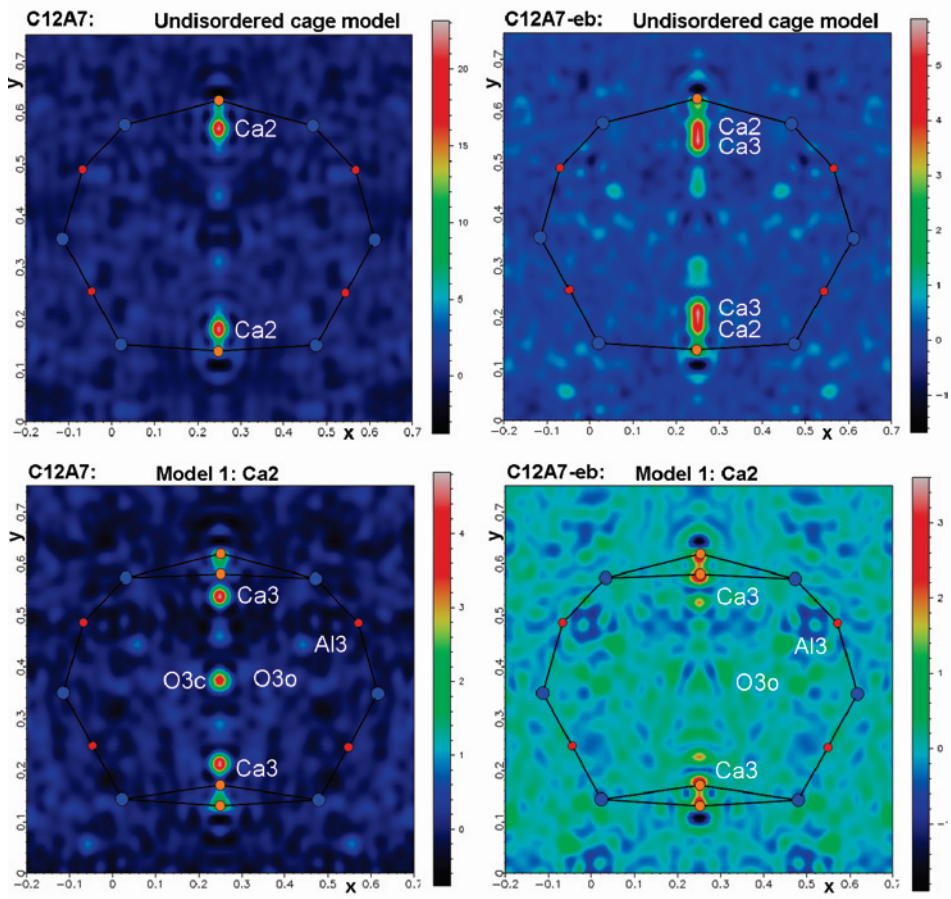


**Figure 3.** Difference Fourier maps in the $x-y$ plane for C12A7 (left) and C12A7-eb (right). Top: maps computed with a nondisordered structural model (Ca1, Al1, Al2, O1, and O2). The most important peak in the C12A7 map is that due to Ca2. The two most important peaks in the C12A7-eb map are those due to Ca2 and Ca3. Bottom: maps computed with an "intermediate" disordered model (Ca1, Ca2 Al1, Al2, O1, O2, and O3o) for C12A7 (left) and C12A7-eb (right). The three most important peaks in the C12A7 map are those due to Ca3, O3c, and Al3 (whose maximum is not in this section). The two most important peaks in the C12A7-eb map are those due to Ca3 and Al3. The maps for C12A7-eg are not given because they are very similar to those of C12A7-eb. The scales range from 22 e $Å^{-3}$ (worst fit) to 3 e $Å^{-3}$ (best fit).

visible. Another peak arising from the oxide anions occluded into the cages, but out of the center, was also observed. However, this peak is masked by the higher intensity of the peaks due to the disorder of the calcium cations, and therefore it is not visualized in the top panels of Figure 3. Hence, an intermediate structural model was developed with the initial model plus Ca2. The electron density peaks due to the disordered calciums, oxides, and aluminum are labeled (bottom panels of Figure 3).

Table 2 gives the site multiplicities, atomic positional parameters, and occupation factors for all atoms in the final structures. Full anisotropic ADPs are given in the Supporting Information (Table S2). The occupation factors of Ca1, Ca2, and Ca3 were refined while constrained to full occupancy of the site, but it must be noted that the Ca2/Ca3 ratio was freely refined. Anisotropic ADPs for Ca1, Ca2, and Ca3 were fixed to be the same to avoid correlations with the refined occupation factors. On the other hand, the occupation factors of Al1 and Al3 were refined, with the same anisotropic ADPs, and also constrained to full occupancy. Finally, the isotropic ADP for O3o, "oxide located out of the center of the cage" (in the three samples), and for O3c, "oxide located at the center of the cage" (for C12A7), was fixed to 0.0061 $Å^2$, also to allow optimization of the occupation factors. This value, 0.0061 $Å^2$, was chosen because it is the average number for the isotropic ADPs of O1 and O2.

The local disorder in the C12A7 sample is somewhat more complex because of the presence of different oxide anion species in the cages, and it will be discussed later. The structural disorder for C12A7-eg and C12A7-eb is the same but differs in magnitude. Figure 2, bottom, depicts the structure of an oxide-occupied cage. The most conspicuous feature is the presence of the O3o oxide anion out of the center of the cage and its structural consequences. In order to fulfill its valence requirements, it provokes the displacement of Ca1 to two new positions, Ca2 and Ca3, with bond distances ranging from 2.33 to 2.34 Å. The presence of two calcium cations is needed in order to have very similar Ca−O3o bond distances along the pseudo-$S_4$ axis. Furthermore, it also provokes 1 Å movement of Al1 to yield Al3, which is bound to O3o. Relevant interatomic distances are given in Table 3, including the cation environment around O3o for all of the samples. The resulting bond valence sum[29] around O3o is close to 1.6 (Table 2). This result is satisfactory for disordered systems. Furthermore, the bond valence sum for the remaining atoms (see Table 2) are also good. We highlight that even the value for Al3 (occupation factor 2–3%) is very good, 2.95. Full lists of bond distances

**Table 2.** Crystallographic Sites, Wyckoff Notation, Positional Parameters, Occupation Factors, and Total Bond Valence Sums for Studied Mayenite Structures

| | C12A7 | C12A7-eg | C12A7-eb |
|---|---|---|---|
| Ca1, ($x$, 0, $^3/_4$), 24d | $x$ = 0.88831(2) | $x$ = 0.88844(3) | $x$ = 0.88847(3) |
| Ca1, occ. factor | 0.769(2) | 0.844(4) | 0.906(4) |
| Ca1, BVS | 1.78 | 1.78 | 1.76 |
| Ca2, ($x$, 0, $^3/_4$), 24d | $x$ = 0.92451(13) | $x$ = 0.9213(5) | $x$ = 0.9200(8) |
| Ca2, occ. factor | 0.1833(9) | 0.0732(8) | 0.044(1) |
| Ca2, BVS | 1.89 | 1.96 | 1.92 |
| Ca3, ($x$, 0, $^3/_4$), 24d | $x$ = 0.9565(4) | $x$ = 0.9582(3) | $x$ = 0.9585(4) |
| Ca3, occ. factor | 0.0457(8) | 0.0778(6) | 0.045(1) |
| Ca3, BVS | 1.69 | 1.67 | 1.66 |
| Al1, ($x$, $x$, $x$), 16c | $x$ = 1.01867(2) | $x$ = 1.01865(3) | $x$ = 1.01801(2) |
| Al1, occ. factor | 0.940(3) | 0.888(2) | 0.936(4) |
| Al1, BVS | 2.74 | 2.71 | 2.70 |
| Al2, (1, $^1/_4$, $^1/_8$), 12b | | | |
| Al2, BVS | 2.89 | 2.89 | 2.87 |
| Al3, ($x$, $y$, $z$), 48e | $x$ = 1.0109(9) | $x$ = 1.0114(7) | $x$ = 1.013(1) |
| | $y$ = −0.0549(9) | $y$ = −0.0525(7) | $y$ = −0.054(1) |
| | $z$ = 1.0552 (9) | $z$ = 1.0548(7) | $z$ = 1.055(1) |
| Al3, occ. factor | 0.0167 (9) | 0.035 (1) | 0.021 (1) |
| Al3, BVS | 2.96 | 2.95 | 2.98 |
| O1, ($x$, $y$, $z$), 48e | $x$ = 0.90049(4) | $x$ = 0.90068(7) | $x$ = 0.90046(5) |
| | $y$ = −0.19231(4) | $y$ = −0.19200(6) | $y$ = −0.19295(5) |
| | $z$ = 0.71388(4) | $z$ = 0.71388(6) | $z$ = 0.71422(5) |
| O1, BVS | 1.94 | 1.93 | 1.93 |
| O2, ($x$, $x$, $x$), 16c | $x$ = 0.93526(3) | $x$ = 0.93522 (6) | $x$ = 0.93474 (5) |
| O2, BVS | 1.65 | 1.64 | 1.64 |
| O3o, ($x$, $y$, $z$), 48e | $x$ = 1.109(2) | $x$ = 1.107(1) | $x$ = 1.143(2) |
| | $y$ = 0.002(2) | $y$ = −0.002(1) | $y$ = 0.062(2) |
| | $z$ = 0.689(2) | $z$ = 0.812(1) | $z$ = 0.753(2) |
| O3o, occ. factor | 0.018 (2) | 0.033 (3) | 0.025(3) |
| O3o, BVS | 1.54 | 1.53 | 1.54 |
| O3c, ($^9/_8$, 0, $^3/_4$), 12b | | | |
| O3c, occ. factor | 0.106(4) | | |

**Table 3.** Selected Interatomic Distances for Studied Mayenite Structures

| | C12A7 | C12A7-eg | C12A7-eb |
|---|---|---|---|
| Ca1 center/Å | 2.833 | 2.833 | 2.836 |
| Ca2 center/Å | 2.400 | 2.440 | 2.459 |
| Ca3 center/Å | 2.017 | 1.997 | 1.997 |
| Al1 center/Å | 3.466 | 3.468 | 3.468 |
| Al3 center/Å | 2.484 | 2.514 | 2.498 |
| O3o center/Å | 0.76 | 0.77 | 0.78 |
| Al3−Al1/Å | 0.99 | 0.96 | 0.98 |
| O3o−Ca2[a]/Å | 2.33(2), *2.70(2)* | 2.34(2), *2.76(2)* | 2.36(2), *2.78(2)* |
| O3o−Ca3[a]/Å | 2.33(2), *1.97(2)* | 2.34(2), *1.93(2)* | 2.34(2), *1.93(2)* |
| O3o−Ca1/Å | 3.28(2) | 3.297(15) | 3.28(2) |
| O3o−Ca1/Å | 3.36(2) | 3.360(15) | 3.36(2) |
| O3o−Al3/Å | 1.73(2) | 1.75(2) | 1.72(2) |
| Al3−O2/Å | 1.701(11) | 1.705(8) | 1.726(12) |
| Al3−O1/Å | 1.687(11) | 1.680(8) | 1.666(12) |
| Al3−O1/Å | 1.854(11) | 1.842(8) | 1.852(12) |
| Al3···O1/Å | 2.749(11) | 2.724(8) | 2.738(12) |
| Al1−O2/Å | 1.7295(8) | 1.7308(12) | 1.7302(11) |
| Al1−O1/Å × 3 | 1.7716(5) | 1.7756(8) | 1.7777(6) |
| Al2−O1/Å × 4 | 1.7401(4) | 1.7409(7) | 1.7434(6) |

[a] The distances given in italics are due to the disorder model, but they are not present in the cages.

and bond valence sums for all possible configurations are given in the Supporting Information (Table S3). It must be underlined that our previous report,[25] with O3o out of the center of the cage but only displacing Ca1 to yield Ca2, gave two O3o−Ca2 distances of 2.18 and 2.30 Å, resulting in a bond valence sum of 0.97, which was unsatisfactory.

It must also be noticed that the position of the "extraframework" oxide out of the center of the cage has been theoretically predicted.[14,30] The same authors also predicted a calcium $S_4$-axis distortion and even aluminum disorder.[30] However, the theoretical calculation gave only one disordered calcium, Ca2, which cannot yield two similar bond distances because O3o is out of the plane perpendicular to the $S_4$ axis. In any case, the derived Ca2···Ca2 distance in the theoretical works, 4.39–4.45 Å (depending upon the selected computational methodology),[14,30] is very similar to the disorder found in this study, with the Ca2···Ca3 distance being 4.44 Å, as inferred by Ca2···center and Ca3···center distances in Table 3. On the other hand, the predicted Al disorder[30] gave a O3o−Al3 bond distance of 2.18 Å, which has been very recently reported at 1.88 Å.[14] We have measured a pronounced disorder, the O3o−Al3 bond length of 1.73 Å (see Table 3). Therefore, the reported structures here will help a fine-tuning of the theoretical calculations.

Once the structure is properly solved, the issue of the electron content can be addressed, which is very challenging in these types of materials. C12A7-eg is green, and it belongs to the series $[Ca_{12}Al_{14}O_{32}]^{2+}\square_{5-\delta}O^{2-}{}_{1-\delta}e^{-}{}_{2\delta}$ with low electron concentration, $2\delta$. This electron concentration can be indirectly determined from three different structural approaches: (I) The refined occupation factor for O3o is 0.033(3), resulting in an extra-framework oxide content of 0.79(7). Therefore, $\delta$ must be close to 0.21, although with a large error because of the low scattering power of the oxide anions for X-rays. (II) The occupation factor for Al3 is directly governed by that of O3o, and it has a much lower error because of its higher scattering power. The occupation factor for Al3 was 0.035(1) and, therefore, $\delta$ must be 0.16(2). (III) O3o also provokes the disorder of the Ca1 cations to give Ca2 and Ca3. The occupation factors should be identical, and the freely refined ratio gave 0.073(1)/0.078(1) (see Table 2). So, taking an average value, 0.075, and its multiplicity, the resulting extraframework oxide content should be 0.90, and so $\delta$ must be 0.10(1). Taking the three independent estimations of the extraframework oxide content, which agree fairly well, the electron loading of C12A7-eg must be close to 0.15 or $n_e \sim 0.34\ 10^{21}$ e cm$^{-3}$.

The electron concentration in C12A7-eb must be much larger than that of C12A7-eg because of the preparation method, the color, and the larger unit cell value. The electron loading, $2\delta$, of C12A7-eb can be indirectly estimated as explained above for C12A7-eg. The refined occupation factor for O3o, 0.025(3), would yield a $\delta$ value close to 0.40. The refined occupation factor for Al3, 0.021(1), would give $\delta$ = 0.49(2). The occupation factors for Ca2/Ca3, 0.044(1)/0.045(1), would imply $\delta$ = 0.47(2). Therefore, these three estimations agree very well, and they give an electron loading for C12A7-eb very close to 0.45 or $n_e \sim 1.0\ 10^{21}$ e cm$^{-3}$, with the maximum electron loading in mayenite being $\delta$ = 1.0 or $n_e = 2.3 \times 10^{21}$ e cm$^{-3}$.[5,23]

The local disorder in C12A7 is slightly more complex because its thermal history (see Experimental Section). The presence of high electron-density scattering at the center of the cages has been modeled by placing an oxide anion at the center of the cage, O3c. This position is an approximation because its scattering is very likely arising from two different contributions: (a) the incorporation of variable contents of $O^{-}{}_2$,[19] $O^{2-}{}_2$,[20] and/or $OH^{-}$[22] anions disordered/vibrating around the center of the cages and (b) the presence of oxide

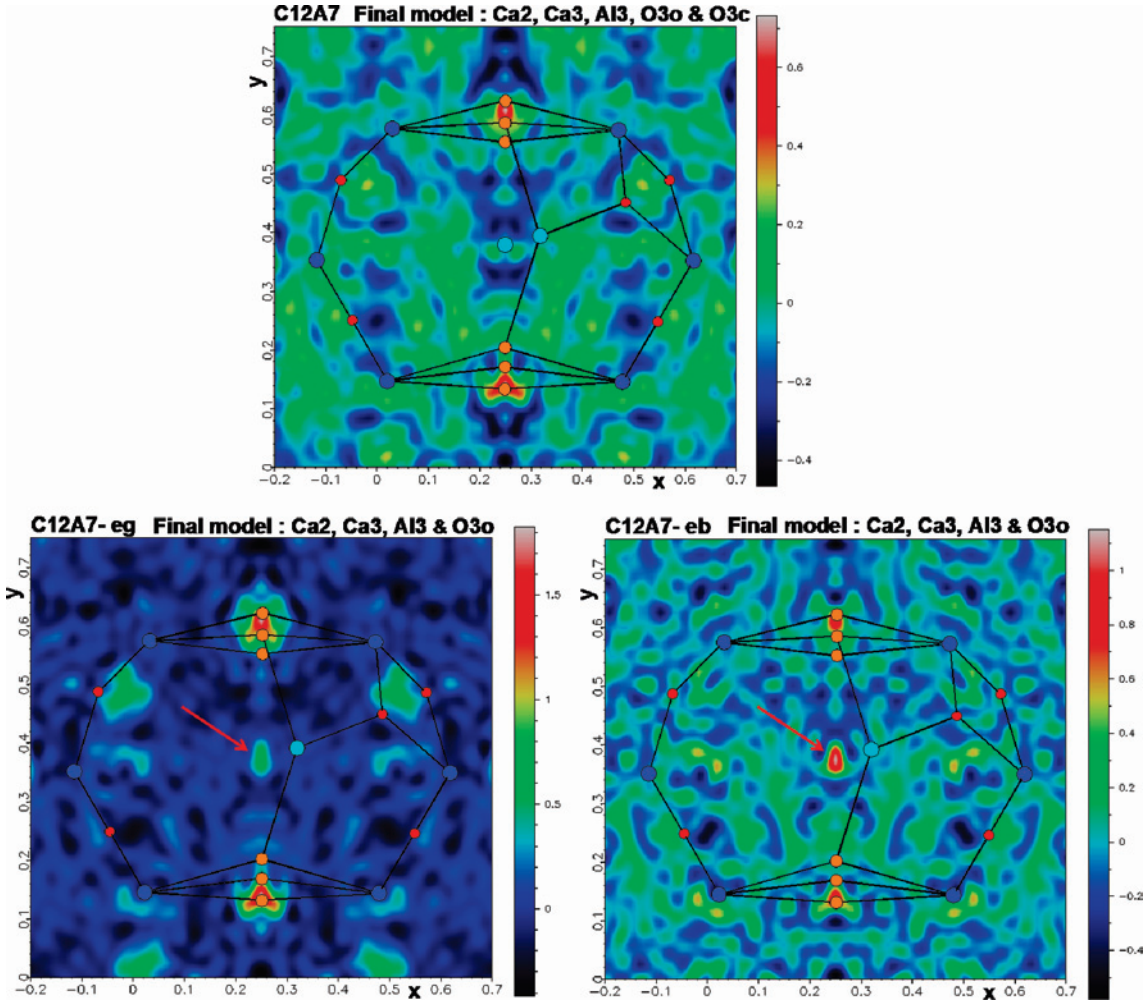


**Figure 4.** Final difference Fourier maps in the $x-y$ plane for C12A7 (top), C12A7-eg (left bottom), and C12A7-eb (right bottom). The maps were computed with the final structural models taking into account the calcium positional disorder (Ca2 and Ca3), the aluminum disorder (Al3), and the oxide disorder (O3o and also O3c for C12A7). There is a residual electron density at the center of the cage for C12A7-eb, underlined with a red arrow, which is probably due to localized electron density in $Ca_{12}Al_{14}O_{32.55}e_{0.9}$. This peak is the most intense peak for C12A7-eb (~1.1 e Å$^{-3}$), and it is also evident in the C12A7-eg map but with much lower intensity (~0.6 e Å$^{-3}$), as was expected for $Ca_{12}Al_{14}O_{32.85}e_{0.3}$. It must be noted that the scales are much smaller (up to 1.2 e Å$^{-3}$) than those given in Figure 3 (up to 22 e Å$^{-3}$).

anions that are not able to coordinate with Al3 because of the occupancy of all neighboring cages, so they are vibrating around the center of the cage and only coordinate to two Ca2 atoms in a loosely bound state. In reduced samples, the oxygen content is lower, and so it is the probability of all first-neighbor cages being occupied. The refined occupation factors for O3c and O3o were 0.106(4) and 0.018(2), respectively. These values yield a refined structural formula of $[Ca_{12}Al_{14}O_{32}]O_{1.07(5)}$. In any case, our disorder model for the oxide anions works well because the refined fraction of the extraframework oxide, O3o (out of the center of the cages) would require an occupation factor of 0.018 for Al3 [the experimental value was 0.017(1) (see Table 2)]. The occupation factors for Ca2 and Ca3 are much larger, and their values depend upon the nature of the oxide species occluded within the cages.

Now we focus on the effects of the electrons into the mayenite structure. It must be noted that the replacement of ~15% of the oxide anions in $Ca_{12}Al_{14}O_{33}$ by electrons in $Ca_{12}Al_{14}O_{32.85}e_{0.3}$ results in a unit cell volume expansion of 0.05% (see Table 1). Furthermore, the volume expansion, 0.21%, is much larger for $Ca_{12}Al_{14}O_{32.55}e_{0.9}$. A second-order effect, likely due to localized electrons, is the very small (but measurable) increase of the Ca2···Ca2 intracage distance. This distortion is 4.88 Å for Ca12A7-eg and increases to 4.92 Å for Ca12A7-eb. This opening of the Ca2···Ca2 intracage distance is compatible with electrons being placed in the center of the cage, and it has been theoretically predicted.[14]

Finally, the accurate modeling of the local disorder and the high quality of the data allow one to have a better insight about the "extraframework" electrons. To do so, Figure 4 plots the difference Fourier maps computed with the final structural models. It is worth noting the improvement in these final models, especially for the C12A7 sample, as there is no peak larger than 0.6 e Å$^{-3}$. The most conspicuous feature is the presence of the highest intense peak at the center of the cages for the black $Ca_{12}Al_{14}O_{32.55}e_{0.9}$ electride. This is the position predicted by theoretical calculations for the electron anions. This peak seems to arise from localized electrons because the same type of map computed with the same model for $Ca_{12}Al_{14}O_{32.85}e_{0.3}$ (see Figure 4) gave no clear

peak, as expected from its lower electron loading. It must be highlighted that the data collection procedure and the structural models are identical for the two samples. It must also be noted that, in the limit of full electron localization, the "extraframework" electron occupation factor for $Ca_{12}Al_{14}O_{32.55}e_{0.9}$ at the center of the cages would be 0.9/6 cages = 0.15. We have tested a model by assuming a hydrogen atom at the center of the cage, with an isotropic ADP of 0.015 Å$^2$, and the refined occupation factor was 0.052(29). The analogous test for $Ca_{12}Al_{14}O_{32.85}e_{0.3}$ gave 0.013(32). Therefore, our diffraction data do not allow one to quantitatively measure the localized electron content. However, the difference Fourier map clearly shows localized electron density in the center of the cages for black $Ca_{12}Al_{14}O_{32.55}e_{0.9}$.

It remains to be investigated how the localized/delocalized fraction of the electron evolves with continuous electron loading, $2\delta$, and, in particular, whether the fully electron-loaded mayenite, $[Ca_{12}Al_{14}O_{32}]^{2+}\square_4\bar{e}_2$, has most of the electrons localized into the center of the cages (electride limit) or most of them delocalized (metallic limit). Our current research is addressing this issue by preparing single crystals with the appropriate electron contents. This type of structural study will clarify the electron behavior in this fascinating family of oxides.

## Conclusions

The crystal structures for three electron-loaded nanoporous mayenite samples, $Ca_{12}Al_{14}O_{33}$, $Ca_{12}Al_{14}O_{32.85}e_{0.3}$, and $Ca_{12}Al_{14}O_{32.55}e_{0.9}$, are reported from single-crystal low-temperature synchrotron X-ray diffraction. The complex structural disorder imposed by the presence of the oxide anions into the mayenite cages has been unraveled. The "extraframework" oxide is located out of the center of the cages, and it provokes the disorder of the calcium cations to give two new sites with equivalent Ca−O bond distances, 2.34 Å, along the pseudo-$S_4$ axis. The "extraframework" oxide also provokes the local displacement of one aluminum atom to give an Al−O bond distance of ∼1.73 Å. The "extraframework" electron contents have been indirectly determined from the three structural approaches with very good agreement. Furthermore, the final electron density map for black $Ca_{12}Al_{14}O_{32.55}e_{0.9}$ mayenite has shown electron density localized into the center of the cages, which is, to the best of our knowledge, the first direct experimental proof of their electride nature.

### Experimental Section

**Synthesis.** Powders of $Ca_{12}Al_{14}O_{33}$ were synthesized by a solid-state reaction between $CaCO_3$ (Alfa Chelometric standard) and $\gamma$-$Al_2O_3$ (Alfa 99.997%) at 1623 K for 16 h in air. These powders were used as raw materials for crystal growth. Mayenite crystals were grown by direct solidification from a melt at 1723 K in a Pt/10% Rh ZGS crucible under an ambient furnace atmosphere. The sample was cooled between 1723 and 1613 K, at 0.1 K min$^{-1}$ rate, and quenched. The greenish-pale transparent crystal was crushed into small pieces and subjected to two different treatments. Some crystals were annealed in air at 1623 K for 1 h and then quenched from 1373 K in a dry atmosphere to avoid the uptake of water and minimize that of oxygen, which mainly takes place in the 1173–773 K temperature range. This procedure yielded the colorless transparent sample labeled as C12A7 (see Figure 1). Other crystals were encapsulated within titanium foils (photograph also shown in Figure 1) and treated at 1273 K under high vacuum ($4 \times 10^{-5}$ mbar) in a silica glass tube holder. The total time of the reductive treatment was 2 days to yield the green crystals labeled as C12A7-eg and 6 days to yield black crystals labeled as C12A7-eb, (see Figure 1).

**Single-Crystal Diffraction.** X-ray diffraction experiments were performed at BM01A beamline of European Synchrotron Research Facility (ESRF), using a multipurpose single-crystal diffractometer KUMA KM6-CH with a 135 mm CCD area detector (Oxford Diffraction, ONYX) and with a crystal-to-detector distance of 100 mm. Diffraction data for the three selected crystals were measured using monochromatic radiation ($\lambda = 0.724\,434$ Å) in an oscillation mode by rotating the crystal in $\varphi$ by 1° in 4–15 s per frame; for each crystal, more than 1500 frames were collected. Data were collected at 90 K by means of an Oxford Cryostream cold nitrogen blower. The intensities were integrated with the program *CrysAlis*.[31] Lorentz polarization and absorption corrections were carried out using *SADABS*[32] up to a 0.45 Å resolution limit. The structure was refined by a full-matrix least-squares technique on $F^2$ using the *SHELXL-97* program,[33] and the missing atoms were located by difference Fourier maps. Data collection details and some crystallographic information are given in Table 1. CIFs files for C12A7, C12A7-eg, and C12A7-eb have been deposited as Supporting Information.

**Acknowledgment.** We thank ESRF (Grenoble, France) for the provision of synchrotron beamtime at BM01A and Dr. Filinchuk for his help during the experiment. Financial support, MAT2006-11080-C02 research grant from MEC, is acknowledged.

**Supporting Information Available:** Table S1 gives the variation of the $R$ factors with the modeled disorder, Table S2 lists the anisotropic ADPs for the final structures, Table S3 reports the full list of bond distances and bond valence sums for all possible configurations in the final structures, and three crystallographic CIF files are also deposited. This material is available free of charge via the Internet at http://pubs.acs.org.

IC7021193

(31) *Xcalibur CCD system, CrysAlisSoftware system*, version 1.171.32; Oxford Diffraction Ltd.: Oxford, U.K., 2005.
(32) *SADABS: Area-Detector Absorption and Other Corrections*, version 2.10; Bruker AXS: Madison, WI, 1997–1999.
(33) Sheldrick, G. M. *SHELXL-97*; University of Gottingen: Gottingen, Germany, 1997.